Energy & Environmental Science

ROYAL SOCIETY OF CHEMISTRY

PAPER

View Article Online
View Journal | View Issue

Cite this: *Energy Environ. Sci.*, 2020, **13**, 5017

Over 14% efficiency all-polymer solar cells enabled by a low bandgap polymer acceptor with low energy loss and efficient charge separation†

Qunping Fan, [a] Qiaoshi An,*[b] Yuanbao Lin,[c] Yuxin Xia, [d] Qian Li,[e] Ming Zhang,[f] Wenyan Su,[agh] Wenhong Peng,[ai] Chunfeng Zhang,[e] Feng Liu, [f] Lintao Hou, [g] Weiguo Zhu, [i] Donghong Yu, [jk] Min Xiao,[e] Ellen Moons, [h] Fujun Zhang, *[l] Thomas D. Anthopoulos, [c] Olle Inganäs[d] and Ergang Wang *[am]

Received 8th June 2020,
Accepted 5th October 2020

DOI: 10.1039/d0ee01828g

rsc.li/ees

Obtaining both high open-circuit voltage (V_{oc}) and short-circuit current density (J_{sc}) has been a major challenge for efficient all-polymer solar cells (all-PSCs). Herein, we developed a polymer acceptor PF5-Y5 with excellent optical absorption capability (onset extending to ~880 nm and maximum absorption coefficient exceeding 10^5 cm^{-1} in a film), high electron mobility (3.18×10^{-3} cm^2 V^{-1} s^{-1}) and high LUMO level (−3.84 eV) to address such a challenge. As a result, the PBDB-T:PF5-Y5-based all-PSCs achieved a high power conversion efficiency of up to 14.45% with both a high V_{oc} (0.946 V) and a high J_{sc} (20.65 mA cm^{-2}), due to the high and broad absorption coverage, small energy loss (0.57 eV) and efficient charge separation and transport in the device, which are among the best values in the all-PSC field. In addition, the all-PSC shows a ~15% improvement in PCE compared to its counterpart small molecule acceptor (Y5)-based device. Our results suggest that PF5-Y5 is a very promising polymer acceptor candidate for applications in efficient all-PSCs.

Broader context

Different from state-of-the-art organic solar cells consisting of p-type polymer donors and n-type small molecule acceptors, all-polymer solar cells (all-PSCs) have such irreplaceable advantages as excellent morphological stability and mechanical robustness, and thus are considered to be more practically compatible with large scale production *via* roll-to-roll printing technology, therefore showing great prospects in their future commercialization. However, the currently reported leading PCEs for almost all all-PSCs in the literature have gained either high open-circuit voltage (V_{oc}) or high short-circuit current density (J_{sc}) only, resulting in unsatisfactory power conversion efficiencies (PCEs), which is mainly due to the lack of high-performance polymer acceptors. Herein, a low bandgap polymer acceptor PF5-Y5 with excellent optoelectronic properties was developed by coupling an electron-deficient benzothiadiazole-fused building block and electron-rich thienyl-benzodithiophene, and the related all-PSCs achieved a high PCE of up to 14.45% with a simultaneously realized high V_{oc} of 0.946 V and high J_{sc} of 20.65 mA cm^{-2}, which are among the best values in the all-PSC field.

[a] *Department of Chemistry and Chemical Engineering, Chalmers University of Technology, Göteborg, SE-412 96, Sweden. E-mail: ergang@chalmers.se*
[b] *School of Chemistry and Chemical Engineering, Beijing Institute of Technology, Beijing 100081, China. E-mail: qsan@bit.edu.cn*
[c] *King Abdullah University of Science and Technology (KAUST), KAUST Solar Center (KSC), Thuwal 23955, Saudi Arabia*
[d] *Biomolecular and Organic Electronics, Department of Physics, Chemistry and Biology (IFM), Linköping University, Linköping, SE-581 83, Sweden*
[e] *National Laboratory of Solid State Microstructures, School of Physics, Collaborative Innovation Center of Advanced Microstructures, Nanjing University, Nanjing 210093, China*
[f] *Department of Physics and Astronomy, Shanghai Jiaotong University, Shanghai 200240, China*
[g] *Guangdong Provincial Key Laboratory of Optical Fiber Sensing and Communications, Guangzhou Key Laboratory of Vacuum Coating Technologies and New Energy Materials, Siyuan Laboratory, Department of Physics, Jinan University, Guangzhou 510632, China*
[h] *Department of Engineering and Physics, Karlstad University, 65188 Karlstad, Sweden*
[i] *School of Materials Science and Engineering, Jiangsu Key Laboratory of Environmentally Friendly Polymeric Materials, Jiangsu Engineering Laboratory of Light-Electricity-Heat Energy-Converting Materials and Applications, Changzhou University, Changzhou 213164, China*
[j] *Department of Chemistry and Bioscience, Aalborg University, DK-9220, Aalborg, Denmark*
[k] *Sino-Danish Center for Education and Research, Aarhus, DK-8000, Denmark*
[l] *School of Science, Beijing Jiaotong University, Beijing 100044, China. E-mail: fjzhang@bjtu.edu.cn*
[m] *School of Materials Science and Engineering, Zhengzhou University, Zhengzhou 450001, China*

† Electronic supplementary information (ESI) available. See DOI: 10.1039/d0ee01828g

Introduction

Recently, tremendous progress in non-fullerene small molecule (SM)-acceptors with a low bandgap (LBG)[1–5] has boosted the power conversion efficiencies (PCEs) of polymer solar cells (PSCs) to over 18%.[6–11] However, recent studies have shown that these SM-acceptors tend to have strong self-aggregation and unsatisfactory mechanical strength, leading to poor morphological stability under heating from long-term solar irradiation or continuous bending.[12,13] Compared to SM-acceptor-based PSCs, all-polymer solar cells (all-PSCs) based on polymer/polymer pairs exhibit highly thermally and mechanically stable morphologies in blends due to strong interchain entanglement and thus are considered to have great potential for practical applications.[13b,14] For example, compared to the PSCs based on SM-acceptor IDIC16, the all-PSCs with an IDIC16-based non-conjugated polymer acceptor PF1-TS4 achieved improved thermal stabilities in both morphology and device performance;[14a] another study indicates that the all-PSCs with an IDIC16-based fully conjugated polymer acceptor PF2-DTSi obtained higher mechanical stabilities in both morphology and device performance in comparison with the polymer:IDIC16 type PSCs.[14b] However, compared to the variety of SM-acceptors, their polymer counterparts have attracted much less attention although the corresponding all-PSCs have some favourable advantages.[14–18] Thus, although very impressive progress has been made in all-PSCs recently, leading to state-of-the-art PCEs improved from 2 to 10–14% within only 7 years,[19–26] they still lag behind those of SM-acceptor-based cells, which is mainly due to the lack of high-performance polymer acceptors.

The structure of the electron-deficient unit has a profound impact on the rational design of polymer acceptors.[26–34] In previous studies, naphthalene diimide-based N2200 was one of the most widely used systems due to its suitable energy levels and good compatibility with donor polymers.[35–38] However, its low absorption coefficient of $\sim 0.3 \times 10^5$ cm^{-1} in films has severely limited the short-circuit current density (J_{sc}) and hence the PCEs of the ensuing all-PSCs.[20,21,36–38] Recently, by inserting a SM-acceptor IDIC-C16 unit with an A–D–A-structured fused-building block, Li *et al.* developed an alternative LBG polymer acceptor PZ1 with a high absorption coefficient ($>10^5$ cm^{-1}).[34] Matching with wide bandgap polymer donors such as PBDB-T or PM6, the resulting all-PSCs showed a high J_{sc} of 16.05–17.1 mA cm^{-2} and impressive PCEs in the range of 9.19–11.2%.[23,34] However, compared to high-performance SM-acceptors with broader absorption spectra and a higher absorption coefficient and thus a high J_{sc} of the resulting PSCs,[1,3,39–42] PZ1 still exhibits limited J_{sc} when implemented in all-PSCs. For example, the SM-acceptor Y5 shows an absorption onset wavelength of $\sim$890 nm with a high absorption coefficient of $\sim 1.24 \times 10^5$ cm^{-1} due to its unique benzothiadiazole (BT)-fused A_1–DA_2D–A_1-type building block.[43] Matching it with PBDB-T, the PSCs achieved a PCE up to $\sim$14% and a high J_{sc} of 22.8 mA cm^{-2}. Moreover, as derivatives of Y5, the tetra-fluorinated Y6[44] and tetra-chlorinated BTP-4Cl[6] achieved higher PCEs ($\sim$16%) and J_{sc} ($\sim$25 mA cm^{-2}) due to their significantly broadened absorption spectra. However, the relatively deep lowest unoccupied molecular orbital (LUMO) levels of these BT-fused SM-acceptors limit the open-circuit voltage (V_{oc}) to 0.83–0.88 V in devices. It has been generally recognized that V_{oc} of devices is roughly proportional to the difference between the HOMO (highest occupied molecular orbital) of the donor and LUMO of the acceptor,[45] which means that up-shifting the LUMO of acceptor materials is the key for improving V_{oc}. Until very recently, only few polymer acceptors based on Y5 derivatives were reported with high PCEs of 11–14% in all-PSCs.[19] It was noticed that these polymer acceptors have excessively long alkyl side-chains in their electron-deficient building block of Y5 derivatives, which may weaken both the interaction and wave function overlap between the Y5 derivative building block of the polymer acceptor and the polymer donor,[46] thus limiting charge transfer in devices and hindering further device performance improvements.[47] Therefore, it is of paramount importance to develop efficient molecular design strategies for novel polymer acceptors with relatively short alkyl side-chains on Y5 derivative building blocks for the sake of improving molecular packing and charge transfer between the donor and acceptor.

Herein, we developed a polymer acceptor PF5-Y5 by introducing Y5 as the electron-deficient unit and thienyl-benzodithiophene (BDT-T) as a donor unit (Fig. 1a). PF5-Y5 shows excellent photoelectric properties with an absorption onset extending to $\sim$880 nm, an absorption coefficient of $>10^5$ cm^{-1}, an electron mobility of 3.18×10^{-3} cm^2 V^{-1} s^{-1}, and a relatively high LUMO level of -3.84 eV. Using PBDB-T as a donor, the PF5-Y5-based all-PSCs achieved an impressively high PCE of 14.45% resulting from a simultaneously increased V_{oc} (0.946 V) and high J_{sc} (20.65 mA cm^{-2}) due to the excellent optical absorption of the active layer, the small energy loss ($\sim$0.57 eV), and efficient charge separation and transport within the devices. The obtained PCE of 14.45% is one of the best values among all-PSCs reported to date and offers a $\sim$15% improvement when compared to its counterpart SM-acceptor (Y5)-based device. Overall, our results indicate that PF5-Y5 is a very promising polymer acceptor candidate for applications in next generation highly efficient all-PSCs.

Results and discussion

PF5-Y5 was synthesized by Stille-coupling polymerization (Scheme S1, ESI†). To avoid potentially strong self-aggregation in films due to the short solubilization side chains and strong π–π stacking of its original SM-acceptor Y5, tetra-alkyl side chain substituted BDT-T for good solubility was introduced as a donor unit into the polymer backbone. Herein, all three batches of the polymer acceptor (PF5-Y5$_{low}$, PF5-Y5$_{medium}$, and PF5-Y5$_{high}$) with weight average molecular weights (M_w) of 16.5, 25.6, and 33.3 kDa, as well as poly-dispersity indexes (PDI) of 2.10, 1.96, and 4.25 (relative to the polystyrene standard), respectively, measured by gel permeation chromatography (GPC) with 1,2,4-trichlorobenzene as an eluent under a high temperature of 150 °C, present good solubility in warm organic solvents such as chloroform and chlorobenzene.

As shown in Table S1 (ESI†), the approximate average number of repeating units of the polymer acceptor was 4, 6, and 4 (while M_w and the PDI are significantly higher than the other two batches) for the three batches, respectively. Since PF5-Y5$_{high}$ shows the highest photovoltaic performance in those three batch polymers, the following discussions focus on PF5-Y5$_{high}$ (also abbreviated as PF5-Y5) in the text below.

Fig. 1b plots the absorption spectra of the active layer materials in films. The acceptors Y5 and PF5-Y5 show similar spectra with strong absorption in the near IR region and an absorption onset of ~880 nm, which match with the wide bandgap donor polymer PBDB-T very well. As a result, the absorption spectrum of the PBDB-T:PF5-Y5 blend film shows full coverage of the high energy region of the solar irradiation spectrum (Fig. S1, ESI†). Moreover, as shown in Fig. S2 (ESI†), the PF5-Y5 neat film displays an improved absorption coefficient of up to ~1.43×10^5 cm^{-1} compared to its SM-acceptor counterpart Y5 (~1.36×10^5 cm^{-1}), which helps the related all-PSCs capture more photons for a higher J_{sc} value. Notably, compared with its SM-acceptor counterpart Y5, PF5-Y5 shows an obviously red-shifted spectrum of ~25 nm in chlorobenzene solution (Fig. S3, ESI†), probably due to the extended conjugation of the polymer backbone, but a slightly blue-shifted spectrum of ~10 nm in a film, which may be attributed to the fact that the introduction of multi-alkyl side chains on BDT-T inhibits the excessive intermolecular aggregation effect of its polymer PF5-Y5 in a film. Compared to the acceptor neat films, the PBDB-T:Y5 blend film shows a similar absorption onset and the PBDB-T:PF5-Y5 blend film displays a slightly blue-shifted absorption onset, which may be due to the fact that the excellent miscibility of PBDB-T and PF5-Y5 weakens the self-aggregation effect of PF5-Y5 in the blend film (discussed right below).

To gain further insights into the difference in molecular crystallinity and packing between SM-acceptor Y5 and polymer acceptor PF5-Y5, grazing incidence wide-angle X-ray scattering (GIWAXS) measurements were performed and the results are shown in Fig. 1c and Fig. S4 (ESI†). Both the acceptors in neat films display a predominant "face-on" orientation, as evidenced by the strong and sharp (010) peaks from π–π stacking in the out-of-plane (OOP) directions. For the lamellar (100) diffraction peaks in the in-plane (IP) profiles, compared to the Y5 neat film with a lamellar distance of 21.99 Å and a crystallite coherence length (CCL) of 46.51 Å, the PF5-Y5 neat film shows a slightly smaller lamellar distance of 18.56 Å but a similar CCL of 45.93 Å. In contrast, for the π–π stacking (010) diffraction peaks in the OOP profiles, the PF5-Y5 neat film displays a dispersive and weak peak with a larger *d*-spacing of 3.82 Å and a decreased CCL of 12.70 Å compared to the Y5 neat film with a sharp and strong peak (the corresponding *d*-spacing is 3.64 Å and the CCL is 20.34 Å). The relatively weak π–π interaction of PF5-Y5 in the neat film observed here indicates that the introduction of multi-alkyl side chains on BDT-T can reduce the strong aggregation effect observed from its SM-acceptor counterpart Y5 in the active layer. This feature explains the slightly blue shifted absorption spectrum observed in the PF5-Y5 film. It is interesting to note that even though PF5-Y5 and Y5 exhibit quite different molecular crystallinity and packing

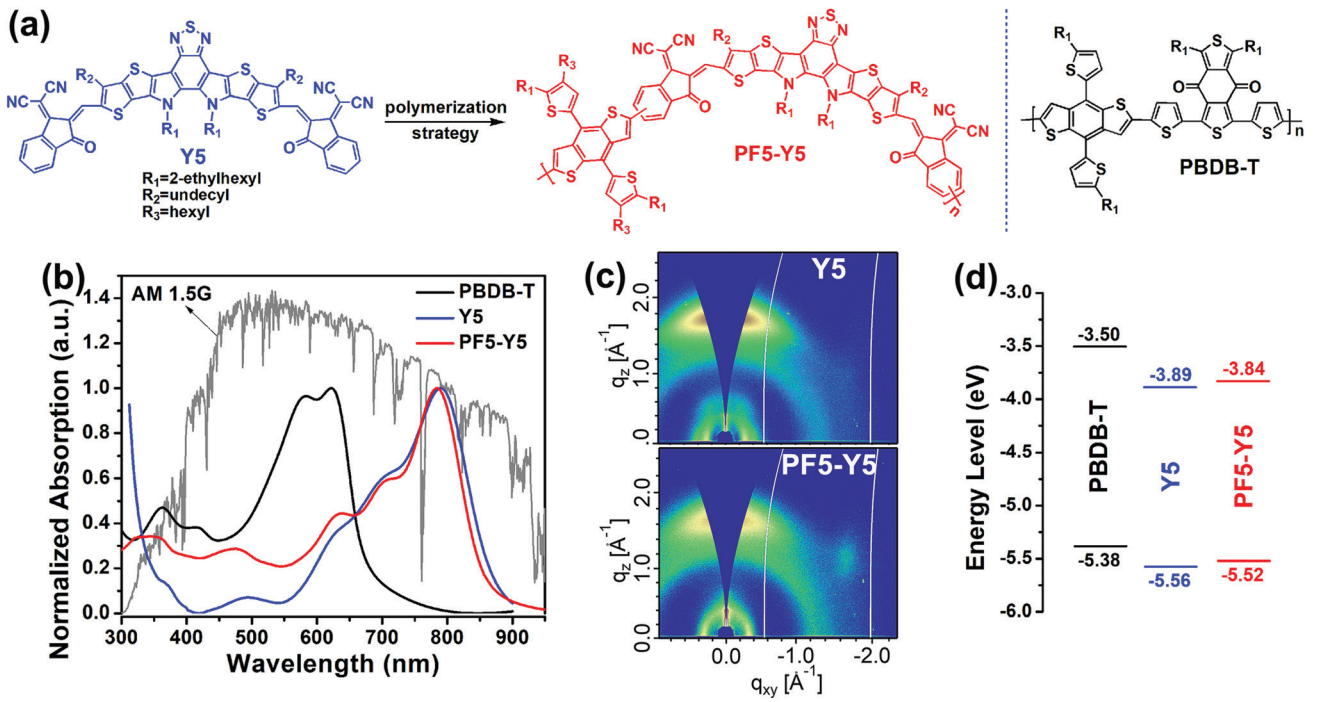

Fig. 1 (a) Chemical structures of the acceptor and donor materials. (b) Normalized absorption spectra of the acceptor and donor materials in neat films. (c) 2D GIWAXS profiles of the acceptors Y5 and PF5-Y5 in neat films. (d) Molecular energy level diagrams measured from neat films using cyclic voltammetry of the acceptor and donor materials.

motifs, the two acceptors yield similar electron mobilities (μ_e) of up to 3.18×10^{-3} cm^2 V^{-1} s^{-1} and 3.82×10^{-3} cm^2 V^{-1} s^{-1}, respectively, as measured by the space charge limited current (SCLC) method (Fig. S5, ESI†). This finding indicates that our polymerization strategy, which relies on combining Y5 with short alkyl side chains and BDT-T with multiple alkyl side chains, does not have any adverse effects on charge transport while inhibiting their excessive self-aggregation effect in films.

Fig. 1d summarises the energy levels of the photovoltaic materials. Compared to its SM-acceptor counterpart Y5 with a LUMO level of −3.89 eV, PF5-Y5 presents an up-shifted LUMO level of −3.84 eV but a still large enough LUMO offset over 0.3 eV relative to PBDB-T, which is beneficial for the corresponding devices to achieve a higher V_{oc}. Moreover, compared to Y5 with a HOMO level of −5.56 eV, PF5-Y5 shows a higher one of −5.52 eV, which is closer to that of the donor PBDB-T (−5.38 eV). As reported, high performance solar cells have been realized from polymer donor:SM-acceptor systems at nearly zero HOMO offset between the donor and the acceptor.[48] The observed small HOMO offset of 0.14 eV between PBDB-T and PF5-Y5 is not naturally expected to hinder efficient exciton dissociation and charge transfer in their all-PSCs, resulting in a low J_{sc} value. Herein, we expect that the new polymer acceptor PF5-Y5 with relatively weak self-aggregation can effectively optimize the blend morphology of PBDB-T:PF5-Y5 by reducing aggregation and phase separation, and then achieve efficient exciton dissociation, charge transfer and charge transport, and eventually high performance in the resulting all-PSCs.

To probe the photovoltaic performance of new polymer acceptor PF5-Y5, all-PSCs with a device structure of ITO/PEDOT:PSS/PBDB-T:PF5-Y5/PDINO/Al were fabricated. The active layer with a thickness of ~100 nm was obtained by spin-coating from a chlorobenzene solution with a total concentration of 17.5 mg mL^{-1}. The D/A ratio of PBDB-T:PF5-Y5 was firstly optimized to be 1 : 0.75. As has been widely recognized, the morphology of the active layers is the key for optimal photovoltaic performance. To achieve this, we used 1-chloronaphthalene (CN) as a solvent additive in combination with thermal annealing post-deposition treatment to optimize the morphology while simultaneously adjusting the active layer composition (*i.e.* D/A ratio). The corresponding optimization processes are summarized in the ESI.† As shown in Fig. S6 and Table S2 (ESI†), the as-cast all-PSCs with an optimal D/A ratio of 1 : 0.75 (w/w) achieved a champion PCE of 12.41% with both a high V_{oc} of 0.922 V and high J_{sc} of 19.89 mA cm^{-2}, which is the highest efficiency reported for as-cast all-PSCs so far. With a small amount of CN additives (v/v, 1–3%) for optimizing the active layer morphology, the all-PSCs exhibited simultaneously improved V_{oc}, J_{sc}, and fill factor (FF), while the 2% CN-processed all-PSC has the highest PCE of 13.61% with a V_{oc} of 0.948 V, a J_{sc} of 20.35 mA cm^{-2}, and a FF of 70.5% (Fig. S7 and Table S3, ESI†). Furthermore, with the active layer treated by thermal annealing at 100 °C for 10 minutes, the all-PSCs achieved an almost constant V_{oc} of 0.944 V, a slightly improved J_{sc} of 20.54 mA cm^{-2}, and an obviously increased FF of 73.1% (Fig. S8 and Table S4, ESI†). As a result, a high PCE of up to 14.16% was achieved in the PBDB-T:PF5-Y5-based all-PSCs (Fig. 2a), which is among the highest PCEs in all-PSCs until now (Fig. 2b and Table S5, ESI†). Notably, as shown in Fig. 2a and Table 1, a similar but slightly higher PCE of 14.45% with a V_{oc} of 0.946 V, a J_{sc} of 20.65 mA cm^{-2}, and a FF of 74.0% was also achieved by Anthopoulos's group at King Abdullah University of Science and Technology (KAUST), which accredited the reliability of our photovoltaic data. Since the photovoltaic performance of all-PSCs could rely on the molecular weights of the polymer acceptors,[19a,b] two additional batches of the polymer acceptor (PF5-Y5$_{low}$ and PF5-Y5$_{medium}$) were synthesized to fully analyze the possible molecular weight dependency of the device efficiency. Our results show irregularly varying J_{sc} and FF, resulting in randomly changed PCEs with no clear molecular weight dependency of the device performance (Fig. S9 and Table S6, ESI†). Meanwhile, contradictory results strongly indicated a huge complexity of such molecular weight effects when comparing the work from Huang *et al.*[19a] and Min *et al.*[19b] The former group claimed a continuous increase from 12.4 to 13.6 and 14.4% of the PCEs for the devices based on the increased molecular weights of 7.3, 11.0, and 23.3 kDa for PJ1-L, PJ1-M, and PJ1-H, respectively, which had been attributed to the molecular weight dependent red-shifted absorption and enhanced extinction coefficient of those three polymers,[19a] while the latter team concluded that a medium-molecular weight PYT$_M$ based device presented the highest PCE due to its highest absorption coefficient/electron mobility and lowest energy loss among PYT$_L$, PYT$_M$, and PYT$_H$.[19b] Therefore, for our PF5-Y5, such molecular weight dependency study needs further detailed investigation in the coming future. The current density–voltage (J–V) plots and the related photovoltaic data of the optimal all-PSCs, as well as the PSCs based on SM-acceptor Y5 for comparison, are summarized in Fig. 2a and Table 1, respectively. The optimization processes of the PBDB-T:Y5-based PSCs are summarized in Fig. S10–S12 (ESI†), which are similar to that of PBDB-T:PF5-Y5, and the corresponding photovoltaic data are listed in Tables S7–S9 (ESI†). Compared to the Y5-based PSCs with a V_{oc} of 0.880 V, a J_{sc} of 19.38 mA cm^{-2}, and a FF of 73.4%, the PF5-Y5-based all-PSCs have a similar FF value but obviously increased V_{oc} and J_{sc}, which results in a ~15% improvement in the PCE. To study the compatibility of PF5-Y5 with other model polymer donors, three representative polymer donors including PCE10,[49] J71,[50] and PM6[51] were used in all-PSCs as well. As shown in Fig. S13 and Table S10 (ESI†), compared to the PBDB-T-based all-PSCs, all of these all-PSCs based on PCE10, J71, and PM6 presented dramatically decreased photovoltaic performance, which may be due to the mismatched molecular energy levels and/or poor morphologies in blend films. In order to further extend our comparison with different acceptors, Y6 was also used as an acceptor in combination with PBDB-T as a donor to fabricate solar cells, leading to a much lower PCE of 8.44% (Fig. S14, ESI†), which is mainly due to the low V_{oc} value of 0.691 V resulting from the mismatched energy levels of the PBDB-T:Y6 pair (Fig. S15, ESI†).

Good thermal stability is one of the key factors for practical application of all-PSCs. As shown in Fig. S16 (ESI†), both of the

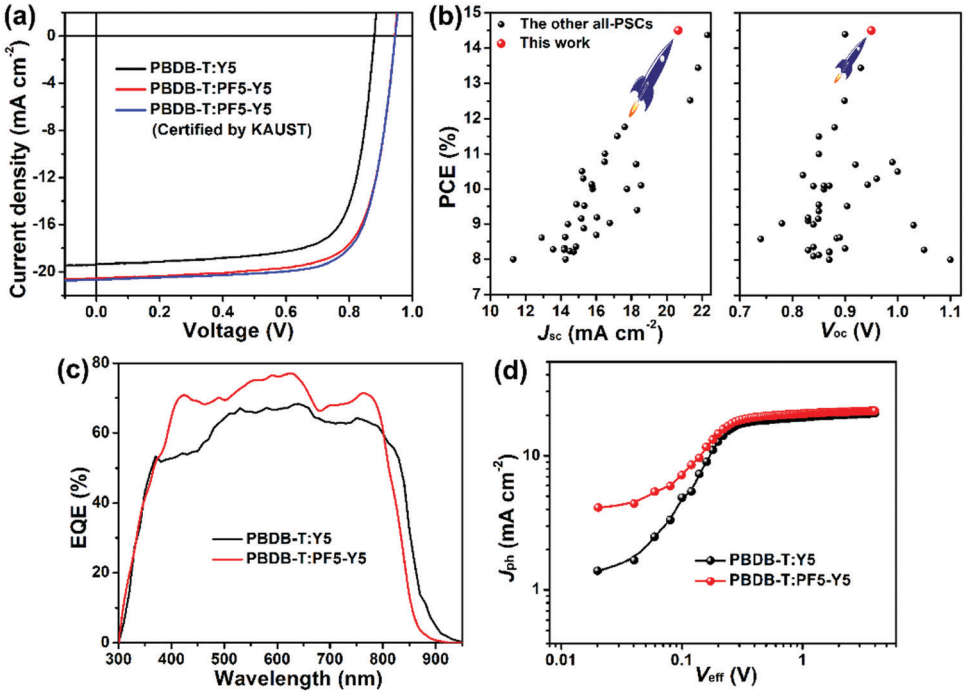

Fig. 2 (a) J–V plots of the PBDB-T:Y5-based PSCs and the PBDB-T:PF5-Y5-based all-PSCs under illumination with AM 1.5G, 100 mW cm^{-2}. (b) Plots of PCE against J_{sc} and PCE against V_{oc} for all-PSCs reported previously with PCEs over 8% and this study. (c) EQE plots of the PBDB-T:Y5-based PSCs and the PBDB-T:PF5-Y5-based all-PSCs, and (d) the corresponding photocurrent density (J_{ph}) *versus* effective voltage (V_{eff}) curves in this study.

Table 1 Summary of key photovoltaic parameters of the PBDB-T:Y5-based PSCs and the PBDB-T:PF5-Y5-based all-PSCs under illumination with AM 1.5G, 100 mW cm^{-2}

Active layers	V_{oc} [V]	J_{sc}[a] [mA cm^{-2}]	FF [%]	PCE[b] [%]
PBDB-T:Y5	0.880	19.38 (19.01)	73.4	12.52 (12.41 ± 0.07)
PBDB-T:PF5-Y5	0.944	20.54 (20.13)	73.1	14.16 (14.03 ± 0.10)
PBDB-T:PF5-Y5[c]	0.946	20.65	74.0	14.45 (14.11 ± 0.26)

[a] The integrated J_{sc} in parentheses from the EQE curves. [b] The average PCEs in parentheses calculated from 20 devices. [c] The devices fabricated at KAUST in Saudi Arabia.

devices based on PBDB-T:Y5 and PBDB-T:PF5-Y5 show poor thermal stability and dramatically decreased PCE under continuous thermal storage of 85 °C in an N_2 atmosphere, which is mainly due to the instability of PDINO (3,3′-(1,3,8,10-tetraoxoanthra[2,1,9-*def*:6,5,10-*d*′*e*′*f*′]diisoquinoline-2,9(1*H*,3*H*,8*H*,10*H*)-diyl)bis(*N*,*N*-dimethylpropan-1-amine oxide)) interfaces. A similar phenomenon was also found in previous work.[19f] To better understand the stability of the all-PSCs under thermal conditions, devices with PNDIT-F3N (poly[(9,9-bis(3′-(*N*,*N*-dimethylamino)-propyl)-2,7-fluorene)-*alt*-5,5′-bis(2,2′-thiophene)-2,6-naphthalene-1,4,5,8-tetracaboxylic-*N*,*N*′-di(2-ethylhexyl)imide]) as the interface layer were also fabricated additionally. As shown in Fig. S17 and Table S11 (ESI†), these devices with PNDIT-F3N as the interface layer show similar photovoltaic performance compared to those devices with PDINO as the interface layer, but the former ones display significantly improved thermal stability (Fig. S16, ESI†). Moreover, the PBDB-T:PF5-Y5-based all-PSC shows better thermal stability in device efficiency compared to the PBDB-T:Y5-based one. The former still retained ~75% of its initial PCE after being stored at 85 °C for more than 2500 min, while the latter only retained ~55% of its initial PCE under the same conditions. The different thermal stabilities of these two systems might be mainly due to the synergistic effects of the morphology evolution and interface attenuation. As shown in Fig. S18 (ESI†) of the atomic force microscopy (AFM) measurements, all the blend films show little variation in roughness from 0.98 to 1.08 nm for PBDB-T:Y5 and from 1.51 to 1.69 nm for PBDB-T:PF5-Y5 under continuous thermal storage of 85 °C in an N_2 atmosphere. Notably, compared to the PBDB-T:Y5 blends, which show a gradually increased size in the fibral structure, the PBDB-T:PF5-Y5 blends show little changes in the fibral structure, which can partly explain why the PBDB-T:PF5-Y5-based devices have better thermal stability.

External quantum efficiency (EQE) measurements were performed to verify the J_{sc} values from J–V measurements. As shown in Fig. 2c, the PF5-Y5-based all-PSC shows a blue-shifted EQE spectrum compared to the Y5-based PSCs, which is consistent with the UV-vis measurements in Fig. 1b and Fig. S1 (ESI†). Moreover, the PF5-Y5-based all-PSC displays high EQE response values in the full absorption spectrum range of both the donor (380–680 nm) and acceptor (680–800 nm) materials, indicating the great contribution to light harvesting from both materials and the success of the strategy using an all-polymer donor and acceptor with complementary absorption spectra in the active layers. Despite the similar absorption from the blends of PBDB-T:PF5-Y5 and PBDB-T:Y5, the all-PSCs based on the former one present relatively higher EQE values in comparison with the latter one, which is most likely attributed to the

improved miscibility between PBDB-T and PF5-Y5 and the reduced tendency to self-aggregate (discussed right below), the combination of which leads to optimal bulk-heterojunction morphology. The integrated J_{sc} values from the EQE curves for the PBDB-T:Y5-based and PBDB-T:PF5-Y5-based devices are 19.01 and 20.13 mA cm^{-2}, respectively, which are consistent with the measured ones from the *J*–*V* plots with a mismatch of less than 3%.

The exciton dissociation probabilities $P(E,T)$ were studied to probe the reason why the PF5-Y5-based all-PSC has higher PCE and J_{sc} values than the Y5-based one.[52] As shown in Fig. 2d and Table S12 (ESI†), under short-circuit and maximum power output conditions, the Y5-based PSC has $P(E,T)$ values of 94.03% and 81.76% estimated from the plots of photocurrent (J_{ph}) *vs.* effective voltage (V_{eff}), while the PF5-Y5-based one shows increased $P(E,T)$ values of 95.00% and 84.04%, respectively, indicating that the all-PSCs exhibit more efficient exciton dissociation and charge extraction, which can partially explain the improved J_{sc}.

To further confirm the efficient hole transfer from PF5-Y5 to PBDB-T in the all-PSCs despite their small HOMO offset of 0.14 eV, herein, the hole transfer dynamics of photo-induced carriers in the all-polymer blend film were probed using femtosecond-resolved transient absorption (TA) spectroscopy measurements under a nitrogen atmosphere.[48b,53] According to the absorption of PBDB-T and PF5-Y5, the pump wavelength was selected as 800 nm. Moreover, according to the results of excitation intensity-dependent measurements of acceptor material pure films under a pump wavelength of 800 nm (Fig. S19, ESI†), an excitation intensity of 1.8 μJ cm^{-2} was selected for the following measurements. The TA spectroscopy and related femtosecond-resolved TA dynamic curves of the pure films and related blend films of the photovoltaic materials are shown in Fig. 3 and Fig. S20 and S21 (ESI†). At the pump wavelength of 800 nm, only PF5-Y5 is excited as confirmed by the absence of a TA signal from the PBDB-T neat film (Fig. S20a, ESI†). As shown in Fig. S21a and b (ESI†), a bleaching signal at 780 nm is shown in both the PF5-Y5 neat film and the all-polymer blend film, which is the ground state bleaching (GSB) of the transition in PF5-Y5. Moreover, the two clear bleaching peaks at 590 and 640 nm displayed in the TA spectrum of the two blend films (Fig. 3) are consistent with the GSB signal from the PBDB-T neat film as measured with excitation at 550 nm (Fig. S20b, ESI†). At the pump wavelength of 800 nm, the bleaching peaks at 590 nm from the blend films appear and rise rapidly, reaching maximum values with a life time of ~18 and ~120 ps for PBDB-T:PF5-Y5 and PBDB-T:Y5, respectively (Fig. 3). Since the PBDB-T neat film cannot be excited at the pump wavelength of 800 nm (Fig. S20a, ESI†), the bleaching peak at 590 nm in the blend film can be naturally assigned to the hole transfer from PF5-Y5 or Y5 to PBDB-T, while the PBDB-T:PF5-Y5 blend shows a faster hole transfer process than PBDB-T:Y5. Therefore, with the excitation of light, more efficient hole transfer can occur in the PBDB-T:PF5-Y5 blend film, which is beneficial for photocurrent generation and thus a higher J_{sc} value. After the hole transfer occurs in the blend film, the electrons and holes are concentrated on the PF5-Y5 and PBDB-T pure domains, respectively. They usually have a smaller overlap in wave functions and it is more difficult for them to recombine compared to the case of the neat films. Therefore, the bleaching peak at 640 nm from the PBDB-T:PF5-Y5 blend film exhibits longer-lived carrier features compared to either the PBDB-T or PF5-Y5 neat films (Fig. S22, ESI†).

To probe the effects of different types of acceptors on the molecular crystallinity and packing of the blend films and gain further understanding of the difference in photovoltaic performance from a morphological point of view, GIWAXS, transmission electron microscopy (TEM), and AFM measurements were carried out. The 2D GIWAXS diffraction images of the PBDB-T-based blend films with different acceptors are shown in Fig. 4a and b, and the corresponding OOP and IP line-cuts and performance parameters are summarized in Fig. 4c and Table S13 (ESI†), respectively. For a clear comparison, the GIWAXS results of the PBDB-T neat film are also summarized in Fig. S23 (ESI†). Both blend films show a predominant "face-on" orientation as evidenced by the strong π–π stacking peaks in the OOP direction. In the OOP direction, the PBDB-T:Y5 blend film shows a (010) peak at the same position of 1.73 Å^{-1} as the Y5 neat film, which implies that the orientation of Y5 dominates the blends; in contrast, the PBDB-T:PF5-Y5 blend

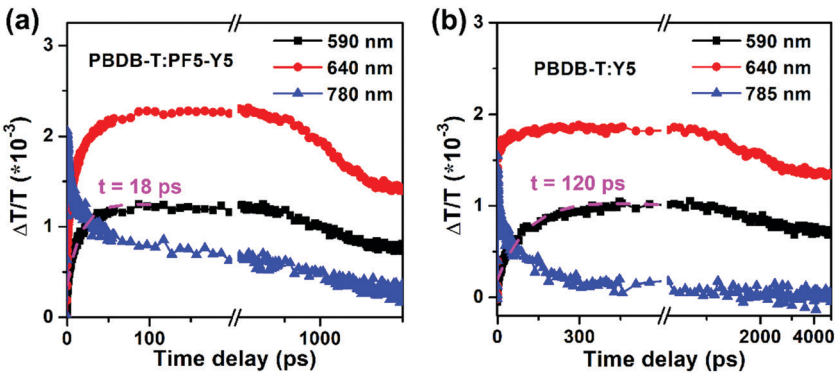

Fig. 3 Femtosecond-resolved transient absorption dynamic curves probed at (a) 590, 640, and 780 nm from the PBDB-T:PF5-Y5 blend film, as well as (b) 590, 640, and 785 nm from the PBDB-T:Y5 blend film.

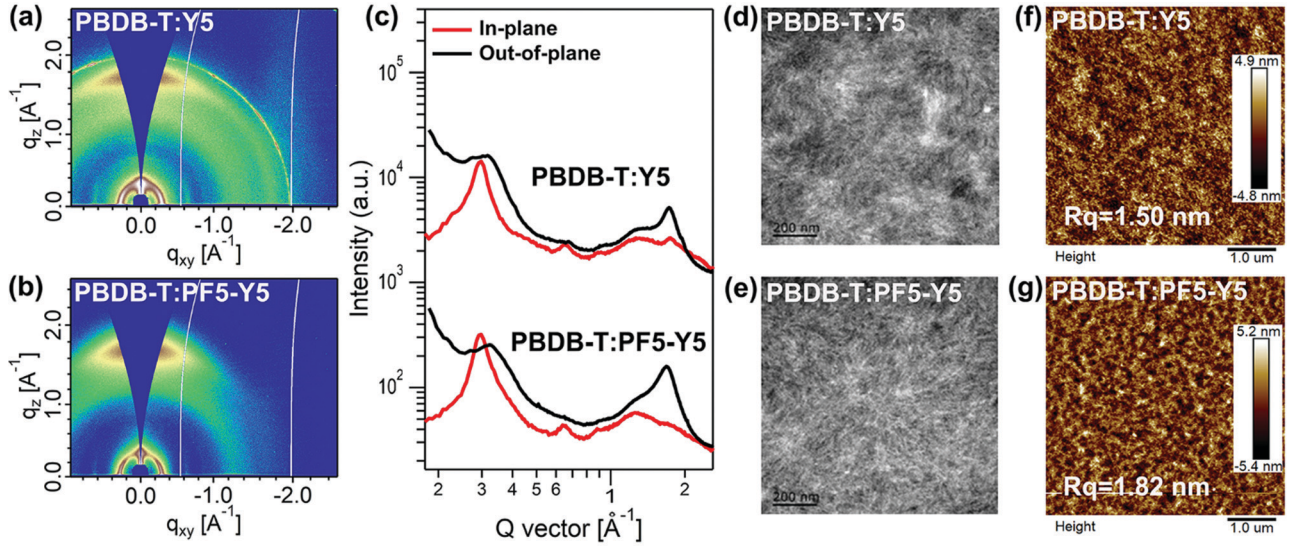

Fig. 4 2D GIWAXS profile of (a) the PBDB-T:Y5 blend film and (b) the PBDB-T:PF5-Y5 blend film, and (c) the corresponding IP and OOP line-cuts from the 2D GIWAXS profiles. TEM images of (d) the PBDB-T:Y5 blend film and (e) the PBDB-T:PF5-Y5 blend film. AFM images of (f) the PBDB-T:Y5 blend film and (g) the PBDB-T:PF5-Y5 blend film.

film has a (010) peak at a similar position of 1.69 Å^{-1} to the PBDB-T neat film, which suggests that the orientation of PBDB-T dominates the blends. Moreover, the PBDB-T:Y5 blend film displays a smaller π–π stacking spacing of 3.63 Å with a higher CCL of 19.16 Å compared to the PBDB-T:PF5-Y5 blend film with a π–π stacking spacing of 3.72 Å and a CCL of 18.04 Å in the OOP direction. For the (100) diffractions belonging to PBDB-T in the IP direction, the PBDB-T:PF5-Y5 blend film shows a higher CCL of 139.7 Å at 0.30 Å^{-1} compared to the PBDB-T:Y5 blend film with a CCL of 124.0 Å at 0.30 Å^{-1}, which indicates that the acceptor polymer PF5-Y5 with reduced crystallinity will not seriously influence the packing of PBDB-T in the blends. Moreover, the PBDB-T:PF5-Y5 blend film displays an additional (100) IP diffraction peak with a small CCL of 53.39 Å at 0.33 Å^{-1} belonging to PF5-Y5 in comparison with the PBDB-T:Y5 blend film. The higher CCL in the (100) diffraction direction of the all-polymer blend film will improve the charge transport and extraction of the corresponding devices,[20] which is consistent with the higher EQE and J_{sc} values from the PBDB-T:PF5-Y5-based all-PSC. As shown in Fig. 4d, the TEM image from the PBDB-T:Y5 blend film shows oversized phase separation in the bulk morphology, which is consistent with the smaller lamellar distance and stronger π–π interaction of Y5 from the GIWAXS results. On the contrary, the PBDB-T:PF5-Y5 blend film has a smaller and more uniform phase separation morphology with a more distinct fibril texture (Fig. 4e), which benefits efficient exciton separation, charge transfer and extraction of the related devices for higher J_{sc} and PCE values. As shown in Fig. 4f and g of the AFM images, both blend films display a small root-mean-square roughness (R_q) of 1.50–1.82 nm, while the PBDB-T:PF5-Y5 blend film has a more uniform fibril texture compared to the PBDB-T:Y5 blend film, which is consistent with the TEM measurements. As shown in Fig. S24 and Table S14 (ESI†), both the PBDB-T:PF5-Y5- and PBDB-T:Y5-based devices achieved high hole and electron mobilities (μ_h and μ_e, ranging from 0.76–2.32 × 10^{-3} cm^2 V^{-1} s^{-1}) with a good balance of μ_h/μ_e values close to 1, which will guarantee efficient charge transport for high performance PSCs.

Since the miscibility of the active layer materials is a key factor to determine the domain size and phase separation of blend films, contact angle measurements were performed to study the interaction between the PBDB-T and acceptor materials, as shown in Fig. S25 (ESI†). According to the Fowkes model,[54] the surface free energy (γ) values of PBDB-T, Y5, and PF5-Y5 are calculated as 24.9, 26.3, and 25.9 mN m^{-1}, respectively. Therefore, the corresponding interaction parameters (χ) of the PBDB-T:Y5 and PBDB-T:PF5-Y5 systems were estimated by the Flory–Huggins method as 2.58 and 2.01, respectively. The weaker interaction between PBDB-T and PF5-Y5 indicates better miscibility between them, and thus a relatively small domain size in their blends is expected, while Y5 shows a stronger interaction with PBDB-T and less miscibility, which is consistent with the TEM results.

To probe why the PF5-Y5-based all-PSC has a notably increased V_{oc} (0.946 V) compared to the Y5-based PSC (0.880 V), we investigated the detailed energy losses of the photovoltaic devices, as shown in Fig. 5 and Table 2. The total voltage loss can be divided into three parts by applying detailed balance theory,[55] as follows:

$$\Delta V_{oc} = \frac{E_g}{q} - V_{oc} = \left(\frac{E_g}{q} - V_{oc}^{SQ}\right) + \left(V_{oc}^{SQ} - V_{oc}^{rad}\right) + \left(V_{oc}^{rad} - V_{oc}\right) = \Delta V_1 + \Delta V_2 + \Delta V_3 \quad (1)$$

Determination of the bandgap (E_g) is problematic, as discussed in ref. 56, so we have chosen to use the method of R_{au}, where E_g is determined by using the derivatives of the EQE, as shown in Fig. 5a. V_{oc}^{SQ} is the maximum voltage based on the Shockley–Queisser (SQ) limit, where several assumptions are made

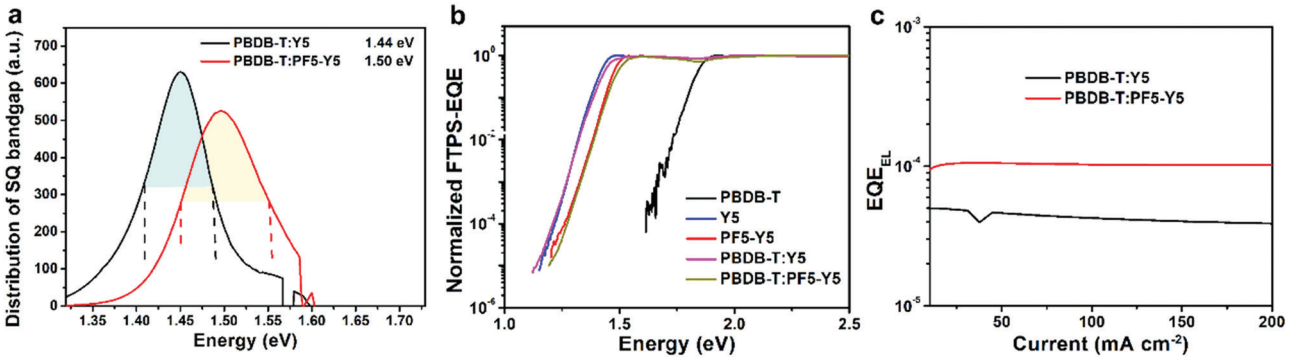

Fig. 5 (a) Distribution of SQ-type bandgaps measured from the derivatives of EQEs in devices, in which the optical bandgap (E_g) of the device is determined from the distribution $P(E)$. (b) Normalized FTPS-EQE curves of the devices based on the pure films and related blend films. (c) EL quantum efficiencies of the devices under different injected currents. The value for the non-radiative loss calculation was chosen when the injection current is close to the short-circuit current under 1 sun irradiation.

Table 2 Detailed V_{oc} losses of the devices based on PBDB-T:Y5 and PBDB-T:PF5-Y5

Active layer	E_g (eV)	V_{oc}^{SQ} (V)	ΔV_1 (V)	ΔV_2 (V)	ΔV_3 (V)	Cal. ΔV_3 (V)	Cal. V_{oc} (V)	E_{loss} (eV)
PBDB-T:Y5	1.44	1.15	0.29	0.03	0.26	0.24	0.86	0.58
PBDB-T:PF5-Y5	1.50	1.20	0.30	0.03	0.24	0.22	0.93	0.57

including the EQE being a step-function and the absence of non-radiative recombination. V_{oc}^{rad} is the open circuit voltage when there is no non-radiative recombination. ΔV_1 can be regarded as the radiative loss and excess kinetic energy loss. ΔV_2 can be regarded as the loss attributed to deviation from a step-function like EQE. ΔV_3 accounts for the non-radiative loss. Calculation of V_{oc}^{rad} requires EQE data in the tail, and therefore highly sensitive Fourier Transform Photocurrent Spectroscopy (FTPS) was performed, as shown in Fig. 5b. More details regarding the calculation can be found in the ESI.†

The estimated E_g for the PBDB-T:PF5-Y5 device is 1.50 eV, which is higher than that (1.44 eV) for the PBDB-T:Y5 device. Based on SQ theory, the V_{oc}^{SQ} values are calculated to be 1.15 V and 1.20 V for the devices based on PBDB-T:Y5 and PBDB-T:PF5-Y5, respectively. Therefore, both devices show similar ΔV_1 values of 0.29–0.30 V. As shown in Fig. 5b, the devices based on PBDB-T:Y5 and PBDB-T:PF5-Y5 show almost the same normalized sensitive-EQE spectra as their corresponding neat acceptor-based devices. Moreover, compared to the acceptor neat films, the corresponding blend films also exhibit similar electroluminescence (EL) spectra without additional emission peaks from the charge-transfer states (Fig. S26, ESI†). The corresponding ΔV_2 values are ~0.03 V for both the PBDB-T:Y5-based and PBDB-T:PF5-Y5-based devices.

ΔV_3 can be estimated by measuring the EQE_{EL} of the devices and using the following equation: $\Delta E_{non\text{-}rad} = -k_B T \ln EQE_{EL}$. As shown in Fig. 5c, the PBDB-T:PF5-Y5-based device shows higher EQE_{EL} values than the PBDB-T:Y5-based one; the corresponding ΔV_3 values are calculated to be 0.24 V for the former and 0.26 V for the latter, respectively. The cal. ΔV_3 values estimated by "$V_{oc}^{rad} - V_{oc}$" are also summarized in Table 2. The decreased non-radiative energy loss is a major contribution to the increase in V_{oc} in the PBDB-T:PF5-Y5-based all-PSCs. As a result, the PBDB-T:PF5-Y5-based all-PSCs achieved a reduced E_{loss} of 0.57 eV and a much higher calculated V_{oc} of 0.93 V compared to the PBDB-T:Y5-based PSCs (E_{loss} = 0.58 eV and a calculated V_{oc} of 0.86 V). The calculated V_{oc} values match well with the measured ones within a negligible error, and its precision is limited by the inadequately precise measuring of EQE data in the low energy region. Therefore, the higher V_{oc} for the PBDB-T:PF5-Y5-based all-PSCs is mainly attributed to the larger bandgap and the smaller non-radiative loss. Notably, the E_{loss} of devices based on the same donor and a structurally similar SM-acceptor and SM-acceptor-based polymeric acceptor was compared directly for the first time. The similar E_{loss} concluded in this work demonstrated that the LBG acceptor polymer developed by our design strategy of polymerization of a SM acceptor and BDT-T units can keep rather low E_{loss} and guarantee high V_{oc} for the resulting all-PSCs, which is a great advantage of all-PSCs and has not been recognized before.

Conclusions

In summary, a new polymer acceptor PF5-Y5 based on BT-fused A_1–DA_2D–A_1 building block Y5 with relatively short alkyl side-chains as an electron-deficient unit and tetra-alkyl side-chain substituted BDT-T as a donor unit was successfully synthesized. PF5-Y5 shows excellent optical absorption characteristics with an absorption onset of ~880 nm and a maximum absorption coefficient of up to 1.43×10^5 cm^{-1}, a high electron mobility of 3.18×10^{-3} cm^2 V^{-1} s^{-1}, an up-shifted LUMO level of −3.84 eV, and suitable molecular crystallinity and packing. As a result, the PF5-Y5-based all-PSCs achieved a high PCE of up to 14.5% with both a high V_{oc} (0.95 V) and a high J_{sc} (20.65 mA cm^{-2}) resulting from the strong optical absorption, the small energy loss (0.57 eV), and the efficient charge separation and transport, which are among the best values in the all-PSC field. Moreover, the all-PSC shows a ~15% improvement in PCE when compared to the Y5-based cells. Our results highlight

PF5-Y5 as a very promising polymer acceptor for applications in efficient all-PSCs.

Author contributions

Q. F., Q. A., and E. W. conceived the idea. Q. F. and W. P. synthesized the photovoltaic materials. Q. A. and F. Z. discussed, fabricated, and optimized the photovoltaic devices. Y. L. and T. D. A. verified and further optimized the photovoltaic performance of all-PSCs. Y. X. and O. I. carried out the energy loss measurements. Q. L., C. Z., and M. X. measured and analysed the T. A. spectra. M. Z. and F. L. characterized the GIWAXS. W. S. and E. M. carried out the AFM measurements. Q. F., W. S., L. H., and W. Z. contributed to the material and device characterization. Q. F., D. Y., and E. W. prepared the manuscript. All authors contributed to editing the manuscript. E. W. supervised and directed the project.

Conflicts of interest

There are no conflicts to declare.

Acknowledgements

We thank the Swedish Research Council (2015-04853, 2016-06146, 2019-04683), the Swedish Research Council Formas, and the Wallenberg Foundation (2017.0186, 2016.0059) for financial support. D. Y. is thankful for the financial support from Innovation fund Denmark (INKA project) and Sino-Danish Centre for Education and Research (SDC). Y. L. and T. D. A. acknowledge support from the King Abdullah University of Science and Technology (KAUST) and Office of Sponsored Research (OSR) under Award No: OSR-2018-CARF/CCF-3079. W. S. is thankful for the project funded by Jinan University Postdoctoral Science Foundation, China Postdoctoral Science Foundation (2020M673054), and National Natural Science Foundation of China (22005121). Q. A. is thankful for the project funded by the National Natural Science Foundation of China (61805009).

Notes and references

1 Y. Lin, J. Wang, Z. Zhang, H. Bai, Y. Li, D. Zhu and X. Zhan, *Adv. Mater.*, 2015, **27**, 1170.

2 (*a*) D. Baran, R. S. shraf, D. A. Hanifi, M. Abdelsamie, N. Gasparini, J. A. Rohr, S. Holliday, A. Wadsworth, S. Lockett, M. Neophytou, C. J. Emmott, J. Nelson, C. J. Brabec, A. Amassian, A. Salleo, T. Kirchartz, J. R. Durrant and I. McCulloch, *Nat. Mater.*, 2017, **16**, 363; (*b*) Q. An, J. Wang, W. Gao, X. Ma, Z. Hu, J. Gao, C. Xu, M. Hao, X. Zhang, C. Yang and F. Zhang, *Sci. Bull.*, 2020, **65**, 538; (*c*) T. Liu, Z. Luo, Q. Fan, G. Zhang, L. Zhang, W. Gao, X. Guo, W. Ma, M. Zhang, C. Yang, Y. Li and H. Yan, *Energy Environ. Sci.*, 2018, **11**, 3275.

3 (*a*) P. Cheng, G. Li, X. Zhan and Y. Yang, *Nat. Photonics*, 2018, **12**, 131; (*b*) X. Che, Y. Li, Y. Qu and S. R. Forrest, *Nat. Energy*, 2018, **3**, 422.

4 (*a*) J. Gao, W. Gao, X. Ma, Z. Hu, C. Xu, X. Wang, Q. An, C. Yang, X. Zhang and F. Zhang, *Energy Environ. Sci.*, 2020, **13**, 958; (*b*) R. Ma, T. Liu, Z. Luo, K. Gao, K. Chen, G. Zhang, W. Gao, Y. Xiao, T.-K. Lau, Q. Fan, Y. Chen, L.-K. Ma, H. Sun, G. Cai, T. Yang, X. Lu, E. Wang, C. Yang, A. K.-Y. Jen and H. Yan, *ACS Energy Lett.*, 2020, **5**, 2711.

5 L. Ye, H. Hu, M. Ghasemi, T. Wang, B. A. Collins, J.-H. Kim, K. Jiang, J. H. Carpenter, H. Li, Z. Li, T. McAfee, J. Zhao, X. Chen, J. L. Y. Lai, T. Ma, J.-L. Bredas, H. Yan and H. Ade, *Nat. Mater.*, 2018, **17**, 253.

6 Y. Cui, H. Yao, J. Zhang, T. Zhang, Y. Wang, L. Hong, K. Xian, B. Xu, S. Zhang, J. Peng, Z. Wei, F. Gao and J. Hou, *Nat. Commun.*, 2019, **10**, 2515.

7 J. Song, C. Li, L. Zhu, J. Guo, J. Xu, X. Zhang, K. Weng, K. Zhang, J. Min, X. Hao, Y. Zhang, F. Liu and Y. Sun, *Adv. Mater.*, 2019, **31**, 1905645.

8 (*a*) Y. Lin, B. Adilbekova, Y. Firdaus, E. Yengel, H. Faber, M. Sajjad, X. Zheng, E. Yarali, A. Seitkhan, O. M. Bakr, A. El-Labban, U. Schwingenschlogl, V. Tung, I. McCulloch, F. Laquai and T. D. Anthopoulos, *Adv. Mater.*, 2019, **31**, 1902965; (*b*) L. Liu, Y. Kan, K. Gao, J. Wang, M. Zhao, H. Chen, C. Zhao, T. Jiu, A.-K.-Y. Jen and Y. Li, *Adv. Mater.*, 2020, **32**, 1907604.

9 (*a*) X. Xu, K. Feng, Z. Bi, W. Ma, G. Zhang and Q. Peng, *Adv. Mater.*, 2019, **31**, 1901872; (*b*) Q. Liu, Y. Jiang, K. Jin, J. Qin, J. Xu, W. Li, J. Xiong, J. Liu, Z. Xiao, K. Sun, S. Yang, X. Zhang and L. Ding, *Sci. Bull.*, 2020, **65**, 272.

10 Z. Zhou, W. Liu, G. Zhou, M. Zhang, D. Qian, J. Zhang, S. Chen, S. Xu, C. Yang, F. Gao, H. Zhu, F. Liu and X. Zhu, *Adv. Mater.*, 2020, **32**, 1906324.

11 (*a*) L. Hong, H. Yao, Z. Wu, Y. Cui, T. Zhang, Y. Xu, R. Yu, Q. Liao, B. Gao, K. Xian, H. Y. Woo, Z. Ge and J. Hou, *Adv. Mater.*, 2019, **31**, 1903441; (*b*) S. Liu, J. Yuan, W. Deng, M. Luo, Y. Xie, Q. Liang, Y. Zou, Z. He, H. Wu and Y. Cao, *Nat. Photonics*, 2020, **14**, 300; (*c*) L. Meng, Y. Zhang, X. Wan, C. Li, X. Zhang, Y. Wang, X. Ke, Z. Xiao, L. Ding, R. Xia, H. L. Yip, Y. Cao and Y. Chen, *Science*, 2018, **361**, 1094.

12 E. M. Speller, A. J. Clarke, J. Luke, H. K. H. Lee, J. R. Durrant, N. Li, T. Wang, H. C. Wong, J.-S. Kim, W. C. Tsoi and Z. Li, *J. Mater. Chem. A*, 2019, **7**, 23361.

13 (*a*) W. Yang, Z. Luo, R. Sun, J. Guo, T. Wang, Y. Wu, W. Wang, J. Guo, Q. Wu, M. Shi, H. Li, C. Yang and J. Min, *Nat. Commun.*, 2020, **11**, 1218; (*b*) Y. Zhang, Y. Xu, M. J. Ford, F. Li, J. Sun, X. Ling, Y. Wang, J. Gu, J. Yuan and W. Ma, *Adv. Energy Mater.*, 2018, **8**, 1800029; (*c*) N. Zheng, K. Mahmood, W. Zhong, F. Liu, P. Zhu, Z. Wang, B. Xie, Z. Chen, K. Zhang, L. Ying, F. Huang and Y. Cao, *Nano Energy*, 2019, **58**, 724.

14 (*a*) Q. Fan, W. Su, S. Chen, T. Liu, W. Zhuang, R. Ma, X. Wen, Z. Yin, Z. Luo, X. Guo, L. Hou, K. Moth-Poulsen, Y. Li, Z. Zhang, C. Yang, D. Yu, H. Yan, M. Zhang and E. Wang, *Angew. Chem., Int. Ed.*, 2019, DOI: 10.1002/ange.202005662; (*b*) Q. Fan, W. Su, S. Chen, W. Kim,

X. Chen, B. Lee, T. Liu, U. A. Méndez-Romero, R. Ma, T. Yang, W. Zhuang, Y. Li, Y. Li, T.-S. Kim, L. Hou, C. Yang, H. Yan, D. Yu and E. Wang, *Joule*, 2020, **4**, 658.

15 (*a*) C. Lee, S. Lee, G. Kim, W. Lee and B. J. Kim, *Chem. Rev.*, 2019, **119**, 8028; (*b*) G. Wang, F. S. Melkonyan, A. Facchetti and T. J. Marks, *Angew. Chem., Int. Ed.*, 2019, **58**, 4129; (*c*) Z.-G. Zhang and Y. Li, *Angew. Chem., Int Ed.*, 2020, DOI: 10.1002/anie.202009666.

16 Z. Genene, W. Mammo, E. Wang and M. R. Andersson, *Adv. Mater.*, 2019, **31**, 1807275.

17 Y. Xu, J. Yuan, S. Zhou, M. Seifrid, L. Ying, B. Li, F. Huang, G. C. Bazan and W. Ma, *Adv. Funct. Mater.*, 2019, **29**, 1806747.

18 J. Yang, B. Xiao, A. Tang, J. Li, X. Wang and E. Zhou, *Adv. Mater.*, 2019, **31**, 1804699.

19 (*a*) W. Wang, Q. Wu, R. Sun, J. Guo, Y. Wu, M. Shi, W. Yang, H. Li and J. Min, *Joule*, 2020, **4**, 1070; (*b*) T. Jia, J. Zhang, W. Zhong, Y. Liang, K. Zhang, S. Dong, L. Ying, F. Liu, X. Wang, F. Huang and Y. Cao, *Nano Energy*, 2020, **72**, 104718; (*c*) A. Tang, J. Li, B. Zhang, J. Peng and E. Zhou, *ACS Macro Lett.*, 2020, **9**, 706; (*d*) J. Du, K. Hu, L. Meng, I. Angunawela, J. Zhang, S. Qin, A. Liebman-Pelaez, C. Zhu, Z. Zhang, H. Ade and Y. Li, *Angew. Chem., Int. Ed.*, 2020, **132**, 15293; (*e*) H. Sun, H. Yu, Y. Shi, J. Yu, Z. Peng, X. Zhang, B. Liu, J. Wang, R. Singh, J. Lee, Y. Li, Z. Wei, Q. Liao, Z. Kan, L. Ye, H. Yan, F. Gao and X. Guo, *Adv. Mater.*, 2020, DOI: 10.1002/adma.202004183; (*f*) Q. Wu, W. Wang, T. Wang, R. Sun, J. Guo, Y. Wu, X. Jiao, C. J. Brabec, Y. Li and J. Min, *Sci. China: Chem.*, 2020, **63**, 1449.

20 L. Zhu, W. Zhong, C. Qiu, B. Lyu, Z. Zhou, M. Zhang, J. Song, J. Xu, J. Wang, J. Ali, W. Feng, Z. Shi, X. Gu, L. Ying, Y. Zhang and F. Liu, *Adv. Mater.*, 2019, **31**, 1902899.

21 (*a*) B. Fan, W. Zhong, L. Ying, D. Zhang, M. Li, Y. Lin, R. Xia, F. Liu, H. L. Yip, N. Li, Y. Ma, C. J. Brabec, F. Huang and Y. Cao, *Nat. Commun.*, 2019, **10**, 4100; (*b*) Z. Li, L. Ying, P. Zhu, W. Zhong, N. Li, F. Liu, F. Huang and Y. Cao, *Energy Environ. Sci.*, 2019, **12**, 157.

22 Q. Fan, R. Ma, T. Liu, W. Su, W. Peng, M. Zhang, Z. Wang, X. Wen, Z. Cong, Z. Luo, L. Hou, F. Liu, W. Zhu, D. Yu, H. Yan and E. Wang, *Solar RRL*, 2020, **4**, 2000142.

23 Y. Meng, J. Wu, X. Guo, W. Su, L. Zhu, J. Fang, Z.-G. Zhang, F. Liu, M. Zhang, T. P. Russell and Y. Li, *Sci. China: Chem.*, 2019, **62**, 845.

24 H. Yao, F. Bai, H. Hu, L. Arunagiri, J. Zhang, Y. Chen, H. Yu, S. Chen, T. Liu, J. Y. L. Lai, Y. Zou, H. Ade and H. Yan, *ACS Energy Lett.*, 2019, **4**, 417.

25 N. B. Kolhe, D. K. Tran, H. Lee, D. Kuzuhara, N. Yoshimoto, T. Koganezawa and S. A. Jenekhe, *ACS Energy Lett.*, 2019, **4**, 1162.

26 R. Zhao, N. Wang, Y. Yu and J. Liu, *Chem. Mater.*, 2020, **32**, 1308.

27 X. Liu, C. Zhang, C. Duan, M. Li, Z. Hu, J. Wang, F. Liu, N. Li, C. J. Brabec, R. A. J. Janssen, G. C. Bazan, F. Huang and Y. Cao, *J. Am. Chem. Soc.*, 2018, **140**, 8934.

28 D. Chen, J. Yao, L. Chen, J. Yin, R. Lv, B. Huang, S. Liu, Z. Zhang, C. Yang, Y. Chen and Y. Li, *Angew. Chem., Int. Ed.*, 2018, **57**, 4580.

29 H. Sun, Y. Tang, C. W. Koh, S. Ling, R. Wang, K. Yang, J. Yu, Y. Shi, Y. Wang, H. Y. Woo and X. Guo, *Adv. Mater.*, 2019, **31**, 1807220.

30 Y. Wu, S. Schneider, C. Walter, A. H. Chowdhury, B. Bahrami, H. C. Wu, Q. Qiao, M. F. Toney and Z. Bao, *J. Am. Chem. Soc.*, 2020, **142**, 392.

31 E. Zhou, M. Nakano, S. Izawa, J. Cong, I. Osaka, K. Takimiya and K. Tajima, *ACS Macro Lett.*, 2014, **3**, 872.

32 Y. Guo, Y. Li, O. Awartani, H. Han, J. Zhao, H. Ade, H. Yan and D. Zhao, *Adv. Mater.*, 2017, **29**, 1700309.

33 S. Liu, X. Song, S. Thomas, Z. Kan, F. Cruciani, F. Laquai, J.-L. Bredas and P. M. Beaujuge, *Adv. Energy Mater.*, 2017, **7**, 1602574.

34 Z.-G. Zhang, Y. Yang, J. Yao, L. Xue, S. Chen, X. Li, W. Morrison, C. Yang and Y. Li, *Angew. Chem., Int. Ed.*, 2017, **129**, 13688.

35 H. Yan, Z. Chen, Y. Zheng, C. Newman, J. R. Quinn, F. Dotz, M. Kastler and A. Facchetti, *Nature*, 2009, **457**, 679.

36 T. Kim, J. H. Kim, T. E. Kang, C. Lee, H. Kang, M. Shin, C. Wang, B. Ma, U. Jeong, T. S. Kim and B. J. Kim, *Nat. Commun.*, 2015, **6**, 8547.

37 N. Zhou, A. S. Dudnik, T. I. Li, E. F. Manley, T. J. Aldrich, P. Guo, H. C. Liao, Z. Chen, L. X. Chen, R. P. Chang, A. Facchetti, C. M. Olvera and T. J. Marks, *J. Am. Chem. Soc.*, 2016, **138**, 1240.

38 J. R. Moore, S. A. Seifried, A. Rao, S. Massip, B. Watts, D. J. Morgan, R. H. Friend, C. R. McNeill and H. Sirringhaus, *Adv. Energy Mater.*, 2011, **1**, 230.

39 J. Lee, S.-J. Ko, M. Seifrid, H. Lee, C. McDowell, B. R. Luginbuhl, A. Karki, K. Cho, T.-Q. Nguyen and G. C. Bazan, *Adv. Energy Mater.*, 2018, **8**, 1801209.

40 X. Du, T. Heumueller, W. Gruber, A. Classen, T. Unruh, N. Li and C. J. Brabec, *Joule*, 2019, **3**, 215.

41 Z. Yao, X. Liao, K. Gao, F. Lin, X. Xu, X. Shi, L. Zuo, F. Liu, Y. Chen and A. K.-Y. Jen, *J. Am. Chem. Soc.*, 2018, **140**, 2054.

42 Q. He, M. Shahid, J. Wu, X. Jiao, F. D. Eisner, T. Hodsden, Z. Fei, T. D. Anthopoulos, C. R. McNeill, J. R. Durrant and M. Heeney, *Adv. Energy Mater.*, 2019, **29**, 1904956.

43 J. Yuan, Y. Zhang, L. Zhou, C. Zhang, T.-K. Lau, G. Zhang, X. Lu, H.-L. Yip, S. K. So, S. Beaupré, M. Mainville, P. A. Johnson, M. Leclerc, H. Chen, H. Peng, Y. Li and Y. Zou, *Adv. Mater.*, 2019, **31**, 1807577.

44 J. Yuan, Y. Zhang, L. Zhou, G. Zhang, H.-L. Yip, T.-K. Lau, X. Lu, C. Zhu, H. Peng, P. A. Johnson, M. Leclerc, Y. Cao, J. Ulanski, Y. Li and Y. Zou, *Joule*, 2019, **3**, 1140.

45 M. C. Scharber, D. Mühlbacher, M. Koppe, P. Denk, C. Waldauf, A. J. Heeger and C. J. Brabec, *Adv. Mater.*, 2006, **18**, 789.

46 K. R. Graham, C. Cabanetos, J. P. Jahnke, M. N. Idso, A. E. Labban, G. O. N. Ndjawa, T. Heumueller, K. Vandewal, A. Salleo, B. F. Chmelka, A. Amassian, P. M. Beaujuge and M. D. McGehee, *J. Am. Chem. Soc.*, 2014, **136**, 9608.

47 (*a*) C. Lee, H. Kang, W. Lee, T. Kim, K.-H. Kim, H. Y. Woo, C. Wang and B. J. Kim, *Adv. Mater.*, 2015, **27**, 2466; (*b*) Y. Cui, H. Yao, L. Hong, T. Zhang, Y. Tang, B. Lin,

K. Xian, B. Gao, C. An, P. Bi, W. Ma and J. Hou, *Nat. Sci. Rev.*, 2020, **7**, 1239; (*c*) D. Mo, H. Chen, J. Zhou, N. Tang, L. Han, Y. Zhu, P. Chao, H. Lai, Z. Xie and F. He, *J. Mater. Chem. A*, 2020, **8**, 8903.

48 (*a*) S. Li, L. Zhan, C. Sun, H. Zhu, G. Zhou, W. Yang, M. Shi, C.-Z. Li, J. Hou, Y. Li and H. Chen, *J. Am. Chem. Soc.*, 2019, **141**, 3073; (*b*) C. Sun, S. Qin, R. Wang, S. Chen, F. Pan, B. Qiu, Z. Shang, L. Meng, C. Zhang, M. Xiao, C. Yang and Y. Li, *J. Am. Chem. Soc.*, 2020, **142**, 1465.

49 S.-H. Liao, H.-J. Jhuo, Y.-S. Cheng and S.-A. Chen, *Adv. Mater.*, 2013, **25**, 4766.

50 H. Bin, L. Gao, Z.-G. Zhang, Y. Yang, Y. Zhang, C. Zhang, S. Chen, L. Xue, C. Yang, M. Xiao and Y. Li, *Nat. Commun.*, 2016, **7**, 13651.

51 (*a*) M. Zhang, X. Guo, W. Ma, H. Ade and J. Hou, *Adv. Mater.*, 2015, **27**, 4655; (*b*) Q. Fan, W. Su, Y. Wang, B. Guo, Y. Jiang, X. Guo, F. Liu, T. P. Russell, M. Zhang and Y. Li, *Sci. China: Chem.*, 2018, **61**, 531; (*c*) Q. Fan, Y. Wang, M. Zhang, B. Wu, X. Guo, Y. Jiang, W. Li, B. Guo, C. Ye, W. Su, J. Fang, X. Ou, F. Liu, Z. Wei, T. C. Sum, T. P. Russell and Y. Li, *Adv. Mater.*, 2018, **30**, 1704546.

52 (*a*) P. W. M. Blom, V. D. Mihailetchi, L. J. A. Koster and D. E. Markov, *Adv. Mater.*, 2007, **19**, 1551; (*b*) J. Gao, J. Wang, Q. An, X. Ma, Z. Hu, C. Xu, X. Zhang and F. Zhang, *Sci. China: Chem.*, 2020, **63**, 83.

53 R. Wang, C. Zhang, Q. Li, Z. Zhang, X. Wang and M. Xiao, *J. Am. Chem. Soc.*, 2020, **142**, 12751.

54 (*a*) F. M. Fowkes, *J. Phys. Chem.*, 1963, **67**, 2538; (*b*) S. Nilsson, A. Bernasik, A. Budkowski and E. Moons, *Macromolecules*, 2007, **40**, 8291.

55 (*a*) U. Rau, B. Blank, T. C. M. Müller and T. Kirchartz, *Phys. Rev. Appl.*, 2017, **7**, 044016; (*b*) X. Ma, J. Wang, J. Gao, Z. Hu, C. Xu, X. Zhang and F. Zhang, *Adv. Energy Mater.*, 2020, **10**, 2001404.

56 Y. Wang, D. Qian, Y. Cui, H. Zhang, J. Hou, K. Vandewal, T. Kirchartz and F. Gao, *Adv. Energy Mater.*, 2018, **8**, 1801352.